Haloalkane Dehalogenase LinB from *Sphingomonas paucimobilis* UT26: X-ray Crystallographic Studies of Dehalogenation of Brominated Substrates[†,‡]

Victor A. Streltsov,*[,§] Zbyněk Prokop,[||] Jiří Damborský,*[,||] Yuji Nagata,[⊥] Aaron Oakley,[§] and Matthew C. J. Wilce*[,§]

Crystallography Centre, School of Biomedical and Chemical Sciences, University of Western Australia, 35 Stirling Highway, Crawley 6009, Western Australia, Australia, National Centre for Biomolecular Research, Masaryk University, Kotlarska 2, 611 37 Brno, Czech Republic, and Graduate School of Life Sciences, Tohoku University, Katahira, Sendai 980-8577, Japan

Received December 2, 2002; Revised Manuscript Received July 6, 2003

ABSTRACT: The haloalkane dehalogenases are detoxifying enzymes that convert a broad range of halogenated substrates to the corresponding alcohols. Complete crystal structures of haloalkane dehalogenase from *Sphingomonas paucimobilis* UT26 (LinB), and complexes of LinB with 1,2-propanediol/1-bromopropane-2-ol and 2-bromo-2-propene-1-ol, products of debromination of 1,2-dibromopropane and 2,3-dibromopropene, respectively, were determined from 1.8 Å resolution X-ray diffraction data. Published structures of native LinB and its complex with 1,3-propanediol [Marek et al. (2000) *Biochemistry 39,* 14082−14086] were reexamined. The full and partial debromination of 1,2-dibromopropane and 2,3-dibromopropene, respectively, conformed to the observed general trend that the sp^3-hybridized carbon is the predominant electrophilic site for the S_N2 bimolecular nucleophilic substitution in dehalogenation reaction. The 2-bromo-2-propene-1-ol product of 2,3-dibromopropene dehalogenation in crystal was positively identified by the gas chromatography−mass spectroscopy (GC−MS) technique. The 1,2-propanediol and 1-bromopropane-2-ol products of 1,2-dibromopropane dehalogenation in crystal were also supported by the GC−MS identification. Comparison of native LinB with its complexes showed high flexibility of residues 136−157, in particular, Asp146 and Glu147, from the cap domain helices α_4 and $\alpha_{5'}$. Those residues were shifted mainly in direction toward the ligand molecules in the complex structures. It seems the cap domain moves nearer to the core squeezing substrate into the active center closer to the catalytic triad. This also leads to slight contraction of the whole complex structures. The flexibility detected by crystallographic analysis is in remarkable agreement with flexibility observed by molecular dynamic simulations.

Major advances in the field of redox enzymes have included the crystal structures of bacterial haloalkane dehalogenase family. The haloalkane dehalogenases act to hydrolyze carbon−halogen bonds where these normally toxic compounds are found in the environment. The haloalkane dehalogenase is a compact globular protein and is a member of the α/β-hydrolase structural superfamily. The α/β-hydrolase superfamily of enzymes is rapidly becoming one of the largest groups of structurally related enzymes with diverse catalytic functions (*1*). Members in this family include acetylcholinesterase, dienelactone hydrolase, lipase, thioesterase, serine carboxypeptidase, proline iminopeptidase, prolyl oligopeptidase, haloalkane dehalogenase, haloperoxidase, epoxide hydrolase, hydroxynitrile lyase, and others. Theses enzymes all have a nucleophile−histidine−acid catalytic triad evolved to efficiently operate on substrates with different physicochemical properties and in various biological contexts. The haloalkane dehalogenases catalyze a replacement reaction in which a primary or secondary halogen of a small molecule substrate is replaced with a hydroxyl group with the associated release of inorganic halide and a proton (*2*). Bimolecular nucleophilic substitution (S_N2) is anticipated reaction mechanism for the carbon−halogen cleavage. The dehalogenase reaction is initiated by the binding of the substrate into a relatively hydrophobic pocket followed by the nucleophilic attack of an aspartic acid residue on the carbon atom to which the halogen is bound. This leads to an alkyl−enzyme intermediate, which is subsequently hydrolyzed by activated water, with a histidine residue acting as a general base. The products are then released. It has been shown that, in fact, the release of the products can be the rate-determining step in the substrate hydrolysis (*3*).

Haloalkane dehalogenase LinB[1] is the enzyme that catalyzes the conversion of 1,3,4,6-tetrachloro-1,4-cyclohexadiene to 2,5-dichloro-2,5-cyclohexadiene-1,4-diol via 2,4,5-trichloro-2,5-cyclohexane-1-ol during γ-HCH dechlorination by *Sphingomonas paucimobilis* UT26 (*4*). In addition to

[†] This work was supported by Australian Research Council and Czech Ministry of Education.

[‡] The atomic coordinates have been deposited to the Brookhaven Protein Data Bank. Reference codes are 1K5P (native LinB), 1K6E (1,2-propanediol/1-bromopropane-2-ol complex), 1K63 (2-bromo-2-propene-1-ol complex), 1IZ7 (re-refined LinB, old code: 1CV2) and 1IZ8 (re-refined 1,3-propanediol complex, old code: 1D07).

* To whom correspondence should be addressed: (V.A.S.) CSIRO HSN 343 Royal Parade, Parkville, VIC 3052, Australia. Fax: (61) 3 96627101. E-mail: victor.streltsov@csiro.au or (J.D.). Fax: (420) 5 41129506. E-mail: jiri@chemi.muni.cz or (M.W.). Fax: (61) 8 93801118. E-mail: mwilce@receptor.pharm.uwa.edu.au.

[§] University of Western Australia.

[||] Masaryk University.

[⊥] Tohoku University.

10.1021/bi027280a CCC: $25.00
Published on Web 08/09/2003

cyclic dienes, LinB also converts a broad range of halogenated alkanes and alkenes to their corresponding alcohols (*5*). The dehalogenation reaction is catalyzed without oxygen or any other cofactor. The amino acid sequence of LinB showed similarity of 28.3% to haloalkane dehalogenase DhlA from *Xanthobacter autotrophicus* GJ10 (*6*, *7*) and of 49.0% to DhaA from *Rhodococcus rhodochrous* NCIMB 13064 (*8*). These three proteins belong to different specificity classes (*9*), which are evolutionary optimized for conversion of different xenobiotic compounds. The structure of DhlA was solved by Dijkstra and co-workers (*10*−*12*), while the structure of DhaA was determined by Newman et al. (*13*). The 1.58 Å crystal structure of LinB and the 2.0 Å structure of LinB with 1,3-propanediol, a product of debromination of 1,3-dibromopropane, in the active site of the enzyme have been determined by Marek et al. (*14*). The 1.8 Å crystal structures of LinB in complex with two substrates, 1,2-dichloroethane and 1,2-dichloropropane, and a reaction product of 1-chlorobutane were analyzed by Oakley et al. (*15*). Complementary structural, kinetic, and gas chromatography−mass spectroscopy (GC-MS) studies for dehalogenation of a series of brominated substrates should provide further information about dehalogenation products, active site topology, interactions with substrate in the protein molecule, and enzyme activity in a crystal and in a solution.

MATERIALS AND METHODS

Crystallization. Haloalkane dehalogenase LinB from *S. paucimobilis* UT26 was overexpressed in *Escherichia coli*, purified to homogeneity, and concentrated to 2.0 mg mL^{-1} in 20 mM potassium phosphate buffer, pH 6.8, with 1 mM of 2-mercaptoethanol, as previously reported (*17*). The enzyme was concentrated to 14.4 mg mL^{-1} by the buffer exchange for 10 mM Tris-HCl pH 7.5, as reported by Smatanova et al. (*18*). Screening for crystallization conditions was performed using commercially purchased sparse-matrix Crystal Screens I and II (Hampton Research, USA) by the hanging drop vapor diffusion technique. All drops were set up by mixing 2 μL of enzyme with 2 μL of precipitant solution on siliconized cover slides and equilibrated against 1 mL of the same precipitant solution. Crystallization trays were incubated at 293 K. In the initial experiments crystals of LinB were obtained using condition 6 of Crystal Screen I (0.2 M magnesium chloride hexahydrate, 30% PEG 4000, 0.1 M Tris hydrochloride, pH 8.5). Condition 6 of Crystal Screen I was considered as an alternative to that given in ref *18* and was attempted for optimization. Condition optimization was performed at 295 K by the hanging-drop and sitting drop variants of the vapor diffusion method using Micro-Bridges in Linbro plates (Hampton Research, USA). Needlelike ~0.5 × 0.1 × 0.1 mm crystals suitable for diffraction analysis formed within 2 days in sitting drops containing 4 μL of protein and 4 μL of reservoir solution with 0.2 M magnesium chloride hexahydrate, 28% PEG 4000 and 0.1 M Tris hydrochloride at pH 8.2. Crystals diffracted up to 1.75 Å resolution.

Table 1: Experimental and Refinement Statistics for LinB Free and LinB−Product Complexes

compounds	LinB	LinB−PGO	LinB−BPO
soak time (min)		60	60
soak temperature (K)		277	277
space group	$P2_12_12_1$	$P2_12_12_1$	$P2_12_12_1$
cell dimensions:	48.286	46.410	46.180
a			
b	68.369	68.330	68.951
c (Å)	80.746	80.980	80.681
molecule dimensions:	48.027	46.349	46.092
x			
y	60.747	60.869	61.456
z (Å)	43.638	43.871	43.768
resolution range (Å)	34.8−1.8	34.7−1.85	27.8−1.8
no. of crystals	1	1	1
no. of unique reflections	21294	21714	23054
completeness of data (%)	83.7(60.3)[a]	95.6(65.0)	93.8(83.5)
I/σ_I	10.6 (2.2)	11.9 (4.7)	11.9(4.0)
multiplicity	4.5 (4.0)	4.5 (4.0)	4.5 (4.0)
R_{merge} (%)	7.7 (28.0)	11.7 (28.1)	11.7(28.0)
refinement statistics:			
protein (non-H)	2328	2328	2328
ligand (non-H)	0	15	10
solvent	423	468	462
ions	5	7	7
R_{factor} (%)	16.6 (29.2)	14.2 (19.1)	14.0 (20.2)
R_{free} (%)	22.6 (32.6)	20.1 (22.7)	19.9 (27.1)
mean B overall ($Å^2$)	15.9	14.8	12.0
RMSD from ideal geometry:			
bonds (Å)	0.014	0.014	0.014
angles (°)	1.7	1.7	1.7
dihedrals (°)	23.1	23.1	23.3
impropers (°)	1.13	1.08	1.09

[a] Values given in parentheses are for the highest resolution shell (2.0−1.8 Å).

Soaking Experiments. The soaking compound (20 μL) was added into a well containing the mother liquor. The cover slip on top was resealed. The halogenated compounds then entered the crystal via vapor diffusion from the reservoir. Soaking was performed for about 4 h at 277 K temperature. Soak times and temperature were chosen similar to soaking conditions of LinB in 1,3-dibromopropane (*14*).

Data Collection. Selected protein crystals were mounted in nylon cryoloops (Hampton Research, USA), immersed in cryoprotectant (0.1 M Tris-HCl, pH 8.2, 0.2 M magnesium chloride hexahydrate, 28% PEG4000, 20% glycerol) for a few seconds, and then rapidly exposed to a cold nitrogen stream (Oxford Cryosystems Cryostream, England). Data were collected at 100 K using a MAR345 area image-plate detector (MarResearch, Germany) and X-rays from a Rigaku RU-200 rotating CuKα anode generator (Rigaku, Japan) operating at 40 kV and 100 mA. X-rays were focused using nickel coated mirrors (MarResearch, Germany). Consecutive batches of 0.2° oscillations were collected. Indexing, integration, and scaling of data sets were carried out using the HKL package (*19*). Present study crystals of LinB from *S. paucimobilis* UT26 diffracted well to 1.8 Å and belong to the orthorhombic space group $P2_12_12_1$ (no. 19). The previously reported crystals (*14*, *18*) were obtained at different conditions and had the orthorhombic space group $P2_12_12$ (no. 18). Data collection details are summarized in Table 1.

Structure Determination and Refinement. The crystal structure of native LinB was solved by the molecular-

[1] Abbreviations: LinB, haloalkane dehalogenase from *Sphingomonas paucimobilis*; DhlA, haloalkane dehalogenase from *Xanthobacter autotrophicus*; DhaA, haloalkane dehalogenase from *Rhodococcus rhodochrous*; LinB−PGO, LinB complex with 1,2-propanediol/1-bromopropane-2-ol; LinB−BPO, LinB complex with 2-bromo-2-propene-1-ol; LinB−PDO, LinB complex with 1,3-propanediol; γ-HCH, γ-hexachlorocyclohexane or lindane; PEG, poly(ethylene glycol); GC-MS, gas chromatography−mass spectroscopy.

replacement method using the CNS package (*20*). As a search model, a previously reported water-free version of native LinB (PDB ID 1CV2) structure was used. The positions of the protein molecule in the asymmetric unit were optimized using the CNS (*20*) rigid-body least-squares refinement using the whole available resolution range. R_{free} cross validation based on randomly selected reflections (10% of the total set) was employed to monitor the subsequent refinement of the model. Following rigid body refinement simulated annealing using torsion angle dynamics was used to improve the model. A starting temperature of 5000 K was used with a cooling rate 50 K per step. To take account of the possible variation in B-factors throughout the model, group B-factors were then refined. Two B-factors were refined for each residue, one for the main-chain atoms and one for the side-chain atoms. After that, both σ_a-weighted *2mFo-DFc* and *mFo-DFc* density maps were calculated and examined using the XtalView program (*21*). The omit maps were used to assist in building the structure. The side chains were adjusted stepwise during the course of refinement using restrained individual B-factor refinement followed by energy minimization of the coordinates. During the final stages of refinement water molecules were inserted into the model only if there were peaks in the *2mFo-DFc* map higher than 2.0 σ with proper hydrogen-bonding distances. Water molecules with displacement factors greater than 80 Å^2 and real space correlation less than 0.5 were excluded from subsequent steps of refinement. The structures of the LinB complexes with products were refined in the manner similar to the native LinB. The starting model was the native LinB structure from the present study with all nonprotein atoms removed. The details of experimental and refinement statistics for LinB free and LinB−product complexes are presented in Table 1.

Identification of Reaction Products by GC-MS. The reaction was started by mixing an enzyme solution (final concentration 3 and 90 μM, respectively) with substrate solution (final concentration 4.81 mM for 1,2-dibromopropane and 4.83 mM for 2,3-dibromopropene) in glycine buffer with pH 8.6. The K_m of LinB with 1,2-dibromopropane is 0.14 mM and with 2,3-dibromopropene is 0.04 mM. The 1 mL of reaction mixture was sampled at 0, 2, 5, 10, 20, 40, 80, 160, 240, and 1020 min of incubation at 37 °C and mixed with 0.5 mL of 0.8 M H_2SO_4 to stop reaction. The quenched samples were then injected into 1 mL of ice-cold diethyl ether. After extraction, the diethyl ether layer containing noncovalently bound substrate and product was separated from the water layer and neutralized by addition of $NaHCO_3$. The water was eliminated by the addition of Na_2SO_4 and diethyl ether was transferred to an autosampler vial for automated analysis. The samples were analyzed using GC-MS Trace MS 2000 (Thermo Finnigan, UK). A total of 5 μL of sample was injected into SSL Injector of Trace GC 2000 (Thermo Finnigan, UK) at 250 °C, with split ratio 25 (split flow was 15 mL min^{-1}). The gas chromatograph was equipped with capillary column DB5-MS 25 m × 0.25 mm × 0.25 μm (J&W Scientific, USA). The temperature program was 3-min isothermal at 60 °C followed by an increase to 140 °C at 20 °C min^{-1}. The flow of carrier gas (He) was 0.6 mL min^{-1} for 3 min followed by an increase to 1.4 mL min^{-1} at 0.2 mL min^{-1} min^{-1}. The MS was operated at SCAN mode with *m*/*z* range from 10 to 220. The temperature of ion source was 200 °C, and the temperature of interface was 250 °C.

RESULTS

Refined Structures. The results of structure refinements are reported in Table 1. The present LinB structure was packed in the unit cell with additional 2-fold screw axis along the *c* direction (sp. gr. $P2_12_12_1$) compared to that determined by Marek et al. (*14*). The electron density was clearly observed for the complete protein structure from N-terminal Ser2 to the C-terminal residue Ala296. Ser2 and Leu3 residues at the N-terminus and side chains for Glu10, Asp73, and Glu145, missing in the initial structure (*14*), were built into the generated density maps. No trace of the electron density for the first Met amino acid in a polypeptide chain was observed. That could indicate either a high level of disorder of the N-terminus or, more likely, that this residue was subject for posttranslational modification. There were several water molecules including that located in the active center with unusually low B-factors of 2.5−4 Å^2. In addition, the residual *mFo-DFc* density maps showed a significant excess density at sites of those waters. Two of he largest peaks were interpreted as the Cl^- ions (a component of the purification and crystallization mixtures). One of them was at the position of the water molecule in the active center close to Asp108 and Trp109 (Figure 1A), and another one on the surface of the molecule. Three other peaks in the intermolecular space were interpreted as Mg^{2+} cations (a component of the crystallization mixture), as they appeared to be coordinated by six water molecules with the average Mg^{2+} to O (water) distances of 2.1 Å. Those were built into the density and included in later rounds of refinement. After refinement the B-factors were in the reasonable ranges of values: 17.4−19.0 and 11.0−19.1 Å for Cl^- and Mg^{2+}, respectively. The final model of native LinB protein contained 2328 non-hydrogen protein atoms, two Cl^- and three Mg^{2+}, and 423 water molecules and converged to *R* and R_{free} of 16.6 and 22.6% for all experimental data (34.8−1.8 Å). Assessment of the quality of the final structure showed that 88.3% of the residues fell in the most favored region, 11.3% were in additional allowed region and Asp108 was in generously allowed regions, and no residues were in disallowed region of the Ramachandran plot. It should be mentioned that Ala247 ϕ angle of −148.8° was very close to the generously allowed region boundary.

In the structures of the LinB−PGO (complex with 1,2-propanediol and 1-bromopropane-2-ol products of 1,2-dibromopropane debromination) and LinB−BPO (complex with 2-bromo-2-propene-1-ol product of 2,3-dibromopropene debromination), the magnesium atoms were observed at the same sites as in the native LinB. The large residual density peaks and small B-factors were obtained for the water placed at the positions attributed to Cl^- in the native LinB. Similar replacement of these waters with the Cl^- ions only was not satisfactory. There was too much electron density of larger volume to be modeled by oxygen or Cl^- ions only. Mixed population of those sites with the Br^- and Cl^- ions: 75:25% for both sites in LinB−PGO, and 60:40% in active site and 40:60% on the surface for LinB−BPO improved significantly the residual density maps and the B-factors, which were increased in average up to 35 and 20 Å for

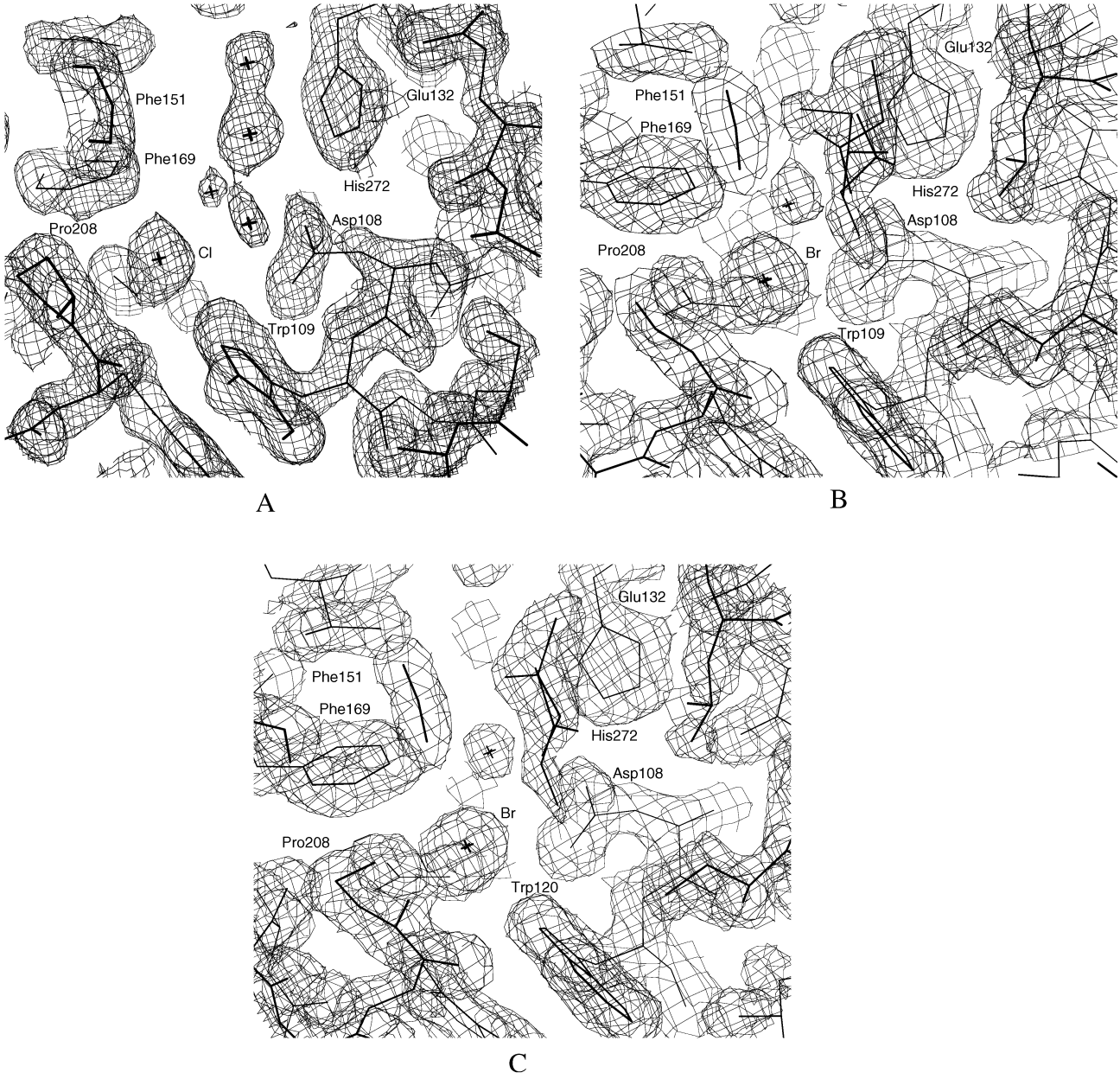

FIGURE 1: The (*2mFo-DFc*) electron density maps, contoured at 1.0 σ level, in the active centers of native LinB (A), LinB−PGO complex (B), and LinB−BPO complex (C).

LinB−PGO and LinB−BPO, respectively. The detection of Br^- in the halide-binding site and the electron density changes in the active site (Figure 1) indicated that the enzyme was active and the dehalogenation took place.

The debromination product models of 1,2-propanediol and 2-bromo-2-propene-1-ol for the LinB−PGO and LinB−BPO complexes, respectively, were built into the electron density in the area close to the nucleophile Asp108 (Figure 1B,C). Bond and angle parameters for the ligands were derived using XPLO2D (*22*) from models produced with WebLab Viewer Pro (Molecular Simulations). However, more electron density than could be accounted for by these ligands or by water molecules as in LinB (Figure 1A) was observed in the area away from Asp108 in the active sites of both complexes. The residual density showed additional significantly high ($>5\sigma$) peaks (two in LinB−PGO and one in LinB−BPO) in those areas. The heights and shapes (extended radii) of those peaks suggested that additional ligands with Br aligned with the peak positions can be inserted. After extensive inspection of the *2mFo-DFc* and *mFo-DFc* maps and refinements of other possible product models the 1-bromopropane-2-ol molecule in two alternate positions with refined occupancies of 30 and 20% were built into the electron density of the LinB−PGO active site (Figure 1B) in addition to the 1,2-propanediol at 50% occupied position close to Asp108. The corresponding released 1.5 Br^- atoms occupied two positions in the structures with occupancies of 0.75 each. The product molecules displaced three water molecules in the active site. The two positions of 1-bromopropane-2-ol molecule were significantly shifted away from Asp108 and only partially overlapped with 1,2-propanediol (Figure 1B). Those two positions were determined by the location of the large electron density peaks best modeled as the Br atoms. One molecule with two Br atoms such as 1,2-dibromopropane substrate could not be properly fitted in the electron density.

FIGURE 2: Overview of the tertiary structure of LinB. α-Helices are purple and mauve, β-sheet is in yellow, β-bridge is in green, turns are in cyan, and coils are in black. Figure was generated by VMD (*26*).

The fact that the cryoprotectant contained glycerol implied the possibility that active sites of the complexes might also be populated by glycerol. Indeed geometry of the glycerol molecule allowed it to be fitted in LinB−PGO active site roughly at the position of 1,2-propanediol. However, it was not enough to accommodate the strong peaks well interpreted as Br. In fact, existence of Br^- ions in the structure both at the halogen-binding site and in the ligand sites suggested that there should be some products of debrominations. The best interpretation was obtained including 1-bromopropane-2-ol into two different positions next to the 1,2-propanediol position which could be in principle shared with glycerol. The intention to keep 1,2-propanediol in the active site was supported by the independent investigations (*14*) which showed 1,3-propanediol product of full debromination of 1,3-dibromopropene in the LinB active site. The soaking conditions were similar, but the cryoprotectant contained no glycerol (20% PEG60000, 10% sucrose, and 10% PEG400). The reexamination of the complex structure from ref *14* described below confirmed that the LinB active center contained a product of full debromination. This supported possibility that the LinB−PGO complex should also include 1,2-propanediol in the active site.

A large volume of electron density was seen in the active site of LinB−BPO with two excess residual density peaks ($>5\sigma$) at almost the middle and at the top of the density cloud in Figure 1C. Similar to the LinB−PGO complex, these peaks had heights and shapes that were better interpreted as the Br atoms, rather than the O atoms. Again those peaks were too close to each other (~3.5 Å) to be interpreted as the two Br atoms from the 2,3-dibromopropene substrate. Also, if the only fully dehalogenated product of 2-propene-1,2-diol was to be fitted to the density, one of oxygen atom would be positioned at the high density peak better modeled with the Br atom. Therefore, the electron density was finally interpreted as the 2-bromo-2-propene-1-ol molecule occupying two positions in the active center with 50% occupancies (Figure 2C). Partial debromination of the 2,3-dibromopropene produced one Br^- in total which was distributed between the halide-binding site and the protein surface.

The final model of LinB−PGO contained 2328 non-hydrogen protein atoms, three Mg^{2+}, two Br^- and two Cl^-, five non-hydrogen atoms for 1,2-propanediol, 10 non-hydrogen atoms for two 1-bromopropane-2-ol molecules and 468 water molecules, and converged to R and R_{free} of 14.2 and 20.1% for all experimental data (34.7−1.85 Å). The final model of LinB−BPO contained 2328 non-hydrogen protein atoms, three Mg^{2+}, two Br^- and two Cl^-, 10 non-hydrogen atoms for two 2-bromo-2-propene-1-ol molecules, and 462 water molecules converging to R and Rfree of 14.0 and 19.9% for all experimental data (27.8−1.8 Å). The Ramachandran plots for LinB−PGO and LinB−BPO showed that, respectively, 89.1 and 89.5% of the non-Gly and non-Pro residues fell in the most favored regions, 10.1 and 9.7% were in additional and two (Asp108 and Ala247) were in generously allowed regions, and no residues were in disallowed regions. However, the Ala247 ϕ angles of −153.1° (LinB−PGO) and −152.7° (LinB−BPO) were just slightly out of the generously allowed regions.

Re-Refined Previously Reported Structures. The fact that the active site of the native LinB structure contained the Cl^- ions stipulated careful reexamination of the previously reported (*14*) LinB structure (PDB ID 1CV2). Analyses of the B-factors and the residual electron density showed that there was significant over 5 σ electron density excess at the water sites (1CV2): 1001 (B = 4 Å^2), 1004 (B = 0 Å^2), 1009 (B = 2.5 Å^2), and 1047 (B = 0 Å^2). The largest peak at the position of water 1001 in the active center was satisfactory interpreted as the Cl^- ion (a component of the purification and crystallization mixtures) similar to the native LinB structure of the present report. Three other peaks at the 1004, 1009, and 1047 water positions in the intermolecular space were interpreted as the Ca^{2+} cations (a component of the crystallization mixture), as they appeared to be coordinated by seven, six and eight oxygen atoms from waters and nearest residues with the average Ca^{2+} to O distances of 2.4, 2.3, and 2.5 Å, respectively. The atomic B-factors and the residual density significantly improved after the new model refinement. The Leu3 residue at the N-terminus, the Glu10, Asp73, and Glu 145 side chains and oxygen for Ala296 missing in the initial structure (*14*) as well as the Glu40 rotamer were built into the generated electron density maps. The final new model of the native LinB protein for the experimental data used in previous study (*14*) contained 2322 non-hydrogen protein atoms, one Cl^-, three Ca^{2+}, and 443 water molecules and converged to lower values than obtained by Marek et al. (*14*) R and R_{free} of 14.0 and 17.8%, respectively.

In this context the complex structure of LinB with 1,3-propanediol (LinB−PDO), a product of full debromination of 1,3-dibromopropane, reported by Marek et al. (*14*) was also reexamined and improved (PDB ID 1D07). As for native LinB (1CV2) the missing Leu3, the side chains for Glu10, Asp73, and Glu145 and the O atom for Ala296 were built in to the density. The second Br^- ion (902) found on the protein surface in the original 1D07 refinement was replaced with the Ca^{2+} ion. Such replacement was justified by improvements in the electron density maps and by the similarity of the Ca^{2+} position to that in the above re-refined 1CV2 structure. The extra two Ca^{2+} position were also added

replacing water molecules at the sites similar to the new 1CV2 model. Although their population was reduced, the density fit and the oxygen coordination suggested that they were likely Ca^{2+} rather than waters. The most important adjustment was related to the position of the 1,3-propanediol ligand. There was significant (greater than 3σ) residual density excess at the Br^- position 901 in the active center as well as near the old 1,3-propanediol position in the original 1D07 structure, which suggested that the Br^- population should probably be 1 (0.71 in 1D07) and the 1,3-propanediol molecule position needed adjustment. Two conformations of 1,3-propanediol with approximately 50:50 population were refined in the new position of the ligand. Part of the old 1,3-propanediol site was occupied by additional water. Other water molecules were further revised: some of them were removed and others were added. The new model did not have any residual density (*mFo-DFc*) greater than 3σ and the *2mFo-DFc* map was satisfactory. The final new model of the LinB−PDO complex structure contained 2322 non-hydrogen protein atoms, five non-hydrogen atoms for 1,3-propanediol, one Br^- and three Ca^{2+}, and 320 water molecules. The model refinement converged to R and R_{free} of 16.6 and 24.8% for the experimental data used in previous study (*14*). This reexamination provided an additional justification of the fact that the 1,2-propanediol product of full dibromination of 1,2-dibromopropane could be observed in the LinB−PGO complex.

Structure of LinB Free. The overall structure of present LinB is very similar to that of Marek et al. (*14*). The molecule is composed of two domains: core domain and smaller cap domain as shown in Figure 1 was well described in previous study (*14*). The core includes a twisted eight-stranded β-pleated sheet, which is framed by α-helices on both sides. The cap domain is made of α-helices only. The best fit by the least-squares method (*21*) between present structure and that of Marek et al. (*14*) re-refined in this study gave the root-mean-square deviation (rmsd) of 0.79 Å. Some residues with flexible side chains have larger (>3.0 Å) rmsd, while the location of active center and especially catalytic triad (Asp108, Glu132, and His272) is highly conserved (triad rmsd 0.25 Å). The nucleophile Asp108 is located on the turn after strand β_5 at the start of the helix α_3, the base His272 is positioned in the turn joining β_8 and α_{11}, and the catalytic Glu132 is located after strand β_6. The secondary structure numbering was adopted from ref *23* as reflecting the most conserved elements. The active site of LinB is further composed of residues Asn38 (the turn between strand β_3 and helix α_1); Asp108 and Trp109 (the turn between strand β_5 and helix α_3); Glu132 and Ile134 (strand β_6 and the turn between strand β_6 and helix α_4); Phe143 and Pro144 (the coil between helices α_4 and $\alpha_{5'}$); Gln146, Asp147, and Phe151 (helix $\alpha_{5'}$); Phe169, Val173, and Leu177 (helix α_6); Trp207, Pro208, and Ile211 (helix α_8 and the following coil); Ala247 and Leu248 (the turn between strand β_7 and helix α_{10}); and His272 and Phe273 (the turn between strand β_8 and helix α_{11}). The Cl^- ion position in the active center is fixed by interactions with Asn38, Trp109, and Pro208 (Figure 2). The distances between Cl^- and N are 3.7, 3.3, and 3.5 Å for Asn38, Trp109, and Pro208, respectively. Furthermore, Asn38 and Trp109 provide the positively charged nitrogen-bound hydrogens for efficient stabilization of the transition state of the first reaction step and catalytic activity of the enzyme. Residues Phe169 (Cz−Cl^- = 3.7 Å), Trp207 (Oz−Cl^-= 4.0 Å and Cβ−Cl^- = 4.1 Å), and Ile211 (Cδ1−Cl^- = 3.9 Å) can provide additional stabilization. The second Cl^- ion was located on the surface of the molecule at the distance of 3.2 Å from N(Ala218) and of 16.5 Å from the first Cl^- ion. Some short distances to the symmetry related protein molecule in the unit cell are Cl^-−Cβ(Asn262) = 3.9 Å, Cl^-−Cα(Pro235) = 4.0 Å, Cl^-−Cβ(Pro235) = 4.0 Å, Cl^-−Cβ(Pro261) = 4.1 Å and Cl^-−N(Asn262) = 4.3 Å.

Structure of the Complex of LinB with 1,2-Propanediol/1-Bromopropane-2-ol (LinB−PGO). The 1,2-dibromopropane compound was previously observed (*16*) to act as a good substrate of LinB with catalytic constant k_{cat} four times lower compared to 1,3-dibromopropane substrate studied by Marek et al. (*14*). The positions of products in the LinB−PGO active site showed that after the partial debromination of 1,2-dibromopropane, the 1-bromopropane-2-ol product was rotated in the extended LinB cavity and subjected to further debromination with the final product of 1,2-propanediol. The first free Br^- was placed between Asn38, Trp109, and Pro208 (Figure 1), partially replacing Cl^- in the LinB structure discussed above. The distances between Br^-(Cl^-) and N are 3.4, 3.3, and 3.5 Å for Asn38, Trp109, and Pro208, respectively. Other close contacts were Trp207 (Oz−Cl^-= 4.1 Å and Cβ−Cl^- = 3.4 Å) and Ile211 (Cδ1−Cl^- = 3.9 Å). The molecule dimensions from Table 1 show that the molecule was compressed about 2 Å in the one (x) direction and was slightly expanded in other two (y and z) directions. However, the major shift of residues happened in the cap domain and in the outer shell of residues from both sides of the core domain along eight-stranded β-pleated sheet, while the internal structure and active site kept preserved (Figure 3).

The overall coordinate rmsd calculated between the LinB and LinB−PGO structures was 0.43 Å, while the catalytic triad rmsd was 0.3 Å with the smallest shift of 0.2 Å for His272. The significant shifts in the region of active site were for residues 136−157 from the coil prior to helix α_4, helix α_4, and helix $\alpha_{5'}$ (rmsd > 0.5 Å) toward the 1,2-propanediol molecule. The rotation of this most flexible part of the structure (residues 136−157) relative to the protein core was insignificant (∼0.9°). The shift affected the turns with residues 212−216 (rmsd > 0.5 Å) between helices α_8 and α_9 which were connected to the flexible region via isolated β-bridge formed by hydrogen bonds such as N(Ile138)−H···O(Pro212) = 3.0 Å, O(Ile138)−H···N(Ala214) = 2.9 Å, O(Ile213)−H···N(Gly215) = 3.0 Å, and O(Ile213)−H···N(Thr216) = 2.9 Å in the native LinB. The 1,2-propanediol was close to residues Asp108 (Oδ1−O1(PGO) = 2.9 Å), Trp109 (Nϵ−O1(PGO) = 4.1 Å), and His272 (Nϵ2−O2(PGO) = 4.1 Å).

Structure of the Complex of LinB with 2-Bromo-2-propene-1-ol (LinB−BPO). The X-ray structural analysis of LinB soaked with 2,3-dibromopropene suggested that the dehalogenation reaction occurred and the product was 2-bromo-2-propene-1-ol indicating the dehalogenation from sp^3-carbon site only. That agreed with previous observation (*24*) that the Br at the sp^3 carbon was predominantly attacked by the enzyme. The 2-bromo-2-propene-1-ol ligand occupied two positions in the active site displacing three water molecules observed in the active site of the native LinB structure.

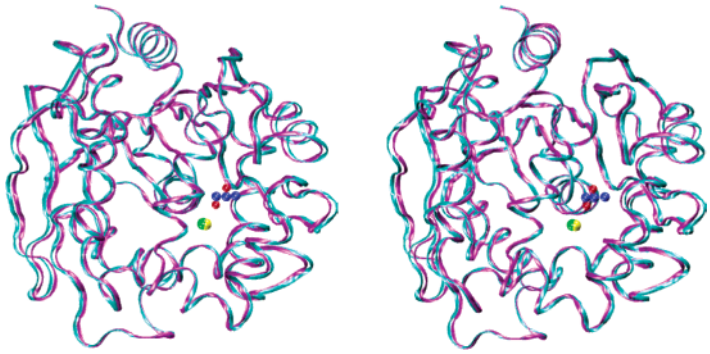

FIGURE 3: Stereo overlay of native LinB (cyan) and LinB−PGO (purple) main chain structures. Positions of ligand and Br^-/Cl^- (green/yellow) are also indicated. Figure was generated by VMD (*25*).

Similar to LinB−PGO complex, the additional position for the 2-bromo-2-propene-1-ol product suggested that after the partial debromination of 2,3-dibromopropene the product could be rotated in the extended LinB cavity and subjected to further debromination. However, it seemed that the full debromination did not occur in the LinB−PGO case.

Comparison of the LinB−PGO structure with the above studied LinB and LinB−PGO structures gave the overall rmsd of 0.51 and 0.23 Å, respectively. The Br:Cl positions were similar to those in the LinB−PGO structure. The distances between Br^- in the active site and N for stabilizing Trp109, Asn38, and Pro208 were 3.3, 3.4, and 3.5 Å, respectively. Other close contacts were Trp207 (Oz−Cl^-= 4.0 Å and Cβ−Cl^- = 4.0 Å), Ile211 (Cδ1−Cl^- = 3.8 Å). The catalytic triad geometry was almost identical in both LinB−PGO and LinB−BPO structures with rmsd of 0.06 Å. The rmsd of catalytic triad in LinB and LinB−BPO was 0.28 Å and close to that for the LinB−PGO. Similar to LinB−PGO, the LinB−BPO structure had also reduced molecule dimension (~2 Å) along the same (*x*) direction (Table 1) due to shift of residues in the cap domain and in the outer shell from both sides of the core domain along eight-stranded β-pleated sheet as in Figure 3. The major shifts in the active site were for residues Asp147 (rmsd 1.3 Å), Glu146 (rmsd 0.9 Å) from helix $\alpha_{5'}$ toward the ligand molecule. As for LinB−PGO, the region between residues 136−157 (coil prior helix α_4, helix α_4 and helix $\alpha_{5'}$) and connected via hydrogen bonds residues 212−216 between helixes α_8 and α_9 in LinB−BPO were also involved in that shift with rmsd >0.5 Å. The 2-bromo-2-propene-1-ol molecule located close the catalytic triad contacted residues Asp108 (Oδ1−O(BPO) = 3.2 Å and Oδ1−C3(BPO) = 2.9 Å), Trp109 (Nϵ1−O(BPO) = 3.9 Å), Ile211 (Cδ1−O(BPO) = 3.9 Å), Leu177 (Cδ1−Br(BPO) = 4.0 Å) and had other longer 4.1−4.5 Å contacts with Ile134, Phe143, Phe151, Leu248 and His272.

Dehalogenation Products of the Substrate 1,2-Dibromopropane. Dehalogenation reaction of LinB with the substrate 1,2-dibromopropane was conducted in the glycine buffer (pH 8.6, t = 37 °C), and the reaction products were studied by GC-MS. The Figure 4A shows dehalogenation of 1,2-dibromopropane (retention time = RT = 4.65 min) and formation of two products (RT = 3.71 and 3.92 min) in time. The mass spectrum of the product at retention time 3.71 min (Figure 4B) was identified as 1-bromopropane-2-ol. Molecular peak with typical cluster M:M+2 in the ratio 1:1 indicates the presence of one bromine atom in the molecule

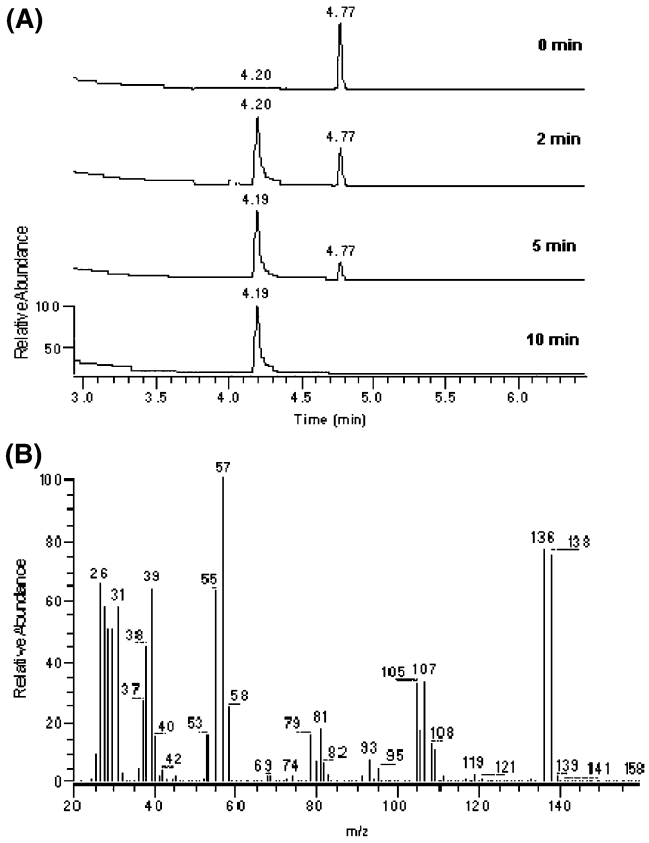

FIGURE 4: Dehalogenation of 1,2-dibromopropane (RT = 4.65 min) and formation of two products (RT = 3.71 and 3.92 min) at 20, 80, and 160 min (A). The mass spectrum of the product with the retention time 3.71 min identified as 1-bromopropane-2-ol (B), with the retention time 3.92 min identified as 2-bromopropane-1-ol (C) and 1,2-propanediol (D). 1,2-Propanediol was identified in the separate experiment conducted at high protein concentration (90 μM) and long reaction time (1020 min).

and corresponds to expected product $C_3H_7BrO^+$ with 138+140 *m*/*z*. Base peak at 45 *m*/*z* represents typical fragment ion from secondary alcohols ($C_2H_5O^+$). The cluster 93+95 *m*/*z* was found in spectrum and identified as remaining ions (CH_2-Br^+) after cleavage of 45 *m*/*z* fragment from molecular ions 138+140 *m*/*z*. NIST/EPA/NIH MS Library search evaluated 95.3% similarity of measured spectra with library spectra of 1-bromopropane-2-ol. The mass spectrum of the product at retention time 3.92 min (Figure 4C) was identified as 2-bromopropane-1-ol. Molecular peak cluster 138+140 *m*/*z* suggests the same molecular formula C_3H_7BrO for this product. There was no sign of ion 45 *m*/*z* typical for secondary alcohols. Peak at 31 *m*/*z* which represents typical

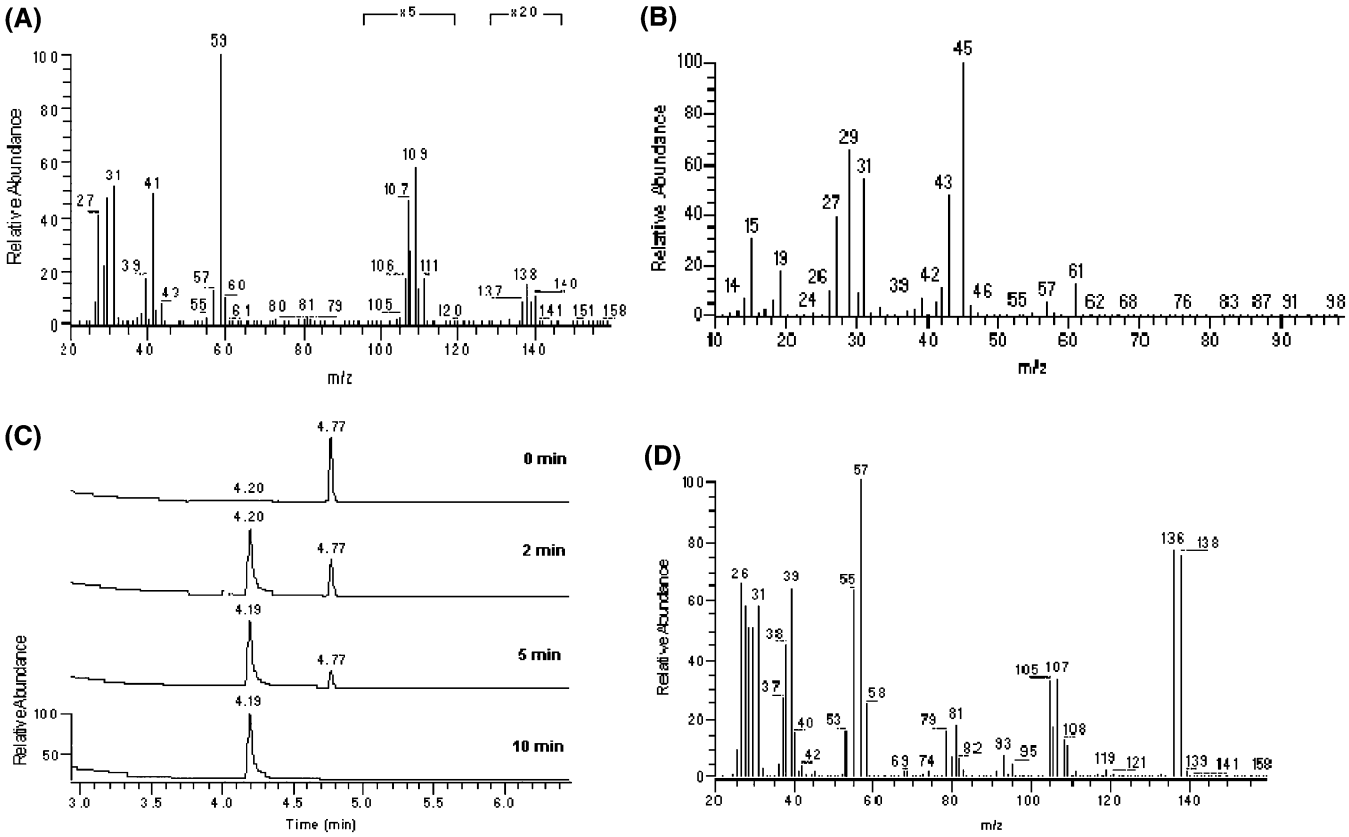

FIGURE 5: Dehalogenation of 2,3-dibromopropene (RT = 4.77 min) and formation of product (RT = 4.20 min) at 2, 5, and 10 min (A). The mass spectrum of the product identified as 2-bromo-2-propene-1-ol (B).

fragment ion from primary alcohols (CH_3O^+) was found in the spectrum. The cluster 107+109 *m*/*z* was found in spectrum and identified as remaining ions ($C_2H_4Br^+$) after cleavage of 31 *m*/*z* fragment from molecular ions 138+140 *m*/*z*. The measured spectra were in good agreement with theoretical fragmentation predicted for 2-bromopropane-1-ol by program MassFrontier 1.0 (HighChem, Slovak Republic). Taken together, these results suggest that LinB enzyme attacks bromine atom of 1,2-dibromopropane at both α- and *β*-position. LinB enzyme preferentially attacks the bromine atom at *β*-position since the rate of 1-bromopropane-2-ol formation was five times faster than formation of 2-bromopropane-1-ol. Dehalogenation experiment conducted at high LinB concentration (90 *μ*M) and long reaction time (1020 min) resulted in a single reaction product. The mass spectra of this product was also identified (Figure 4D). The peak of *m*/*z* 61 corresponds to $C_2H_5O_2$ as a possible fragment of 1,2-propanediol. The typical fragment for primary and secondary alcohols are *m*/*z* 31 and 45, respectively, and both were found in the spectrum. The results suggest that the final product of LinB 1,2-dibromopropane conversion is 1,2-propanediol. NIST/EPA/NIH MS Library search evaluated 78.1% similarity of measured spectra with library spectra of 1,2-propanediol.

Dehalogenation Product of the Substrate 2,3-Dibromopropene. Dehalogenation of 2,3-dibromopropene by LinB was conducted in the glycine buffer (pH 8.6, $t = 37$ °C), and the reaction product was identified using GC-MS. Figure 5A shows dehalogenation of 2,3-dibromopropene (RT = 4.77 min) and formation of product (RT = 4.20 min) in time. The mass spectrum of the product (Figure 5B) was identified as 2-bromo-2-propene-1-ol. Molecular peak with typical cluster M:M+2 in the ratio 1:1 indicates the presence of one bromine atom in the molecule and corresponds to expected product $C_3H_5BrO^+$ with 136+138 *m*/*z*. Peak at 31 *m*/*z* which represents typical fragment from primary alcohol (CH_3O^+) was found in the spectrum. The cluster 105+107 *m*/*z* was found in spectrum and identified as remaining ions ($C_2H_2Br^+$) after cleavage of 31 *m*/*z* fragment from molecular ions 136+138 *m*/*z*. The measured spectrum was in good agreement with theoretical fragmentation predicted by the use of MassFrontier (HighChem, Slovak Republic). There was no other product found in the reaction mixture strongly suggesting that LinB enzyme attacks bromine atom of 2,3-dibromopropene at α-position only.

DISCUSSION

The present structures of LinB and complexes LinB−PGO and LinB−BPO were solved to 1.8 Å resolution by molecular replacement technique. Crystallographic data are summarized in Table 1. The LinB−PGO and LinB−BPO structures were compared with the structure of LinB-1,3-propanediol complex (LinB−PDO), a product of debromination of 1,3-dibromopropane (*14*) re-refined in the present study (PDB ID 1IZ8). The LinB−PGO and LinB−BPO complexes were superimposed on LinB−PDO with the rms deviations of 0.74 and 0.77 Å, respectively. The greatest divergences between the structures were at the N- and C-termini, which were relatively flexible in the structures. The catalytic triad residues superimposed closely with the rmsd's of 0.23 Å in both cases. The 1,2-propanediol and 2-bromo-2-propene-1-ol ligands were approximately superimposed on one another and located slightly closer to the Asp108 than 1,3-propanediol. The hydroxy groups of 1,2-propanediol and

2-bromo-2-propene-1-ol are 2.9 and 3.2 Å away from Asp108-Oδ1, respectively, as opposed to 3.5 Å in the case of 1,3-propanediol. All three ligands were adjacent to the face of the His272 side chain; however, the 1,3-propanediol molecule was found to be shifted approximately in the direction parallel to the face of the His272 roughly toward Pro144 (the OH−Pro144−O distance is 3.2 Å). Superposition of LinB complexes with 1,2-dichloropropane, 1,2-dichloroethane, and butanol, the last one being the product of dechlorination of 1-chlorobutane from the study of Oakley et al. (*15*) as well as with reexamined 1,3-propanediol of Marek et al. (*14*), and 1,2-propanediol/1-bromopropane-2-ol and 2-bromo-2-propene-1-ol from the present study, showed that the ligands were distributed along the same direction approximately from Asp108 to the space between Pro144, Gln146, and Asp147.

It is interesting to note that while the ligand positions are stretched along the direction parallel to the face of the His272, the catalytic triad approached the ligands from the core side of the protein with their active atoms approximately arranged in the plane, which is almost parallel to the face of the His272 imidazole side chain. From the opposite side, the ligands are approached by the most flexible residues 143−151 from the cap domain helices α_4 and $\alpha_{5'}$. The latter residues and especially, Asp146 and Glu147, are mainly shifted toward the ligand molecules in the LinB−PGO and LinB−BPO structures. It suggests that the cap domain moves closer to the core squeezing substrate in the active center and bringing it closer to the catalytic triad. This is reflected on the dimensions of the molecules (Table 1) as mentioned above. This agrees with molecular dynamics simulation (*23*), which showed that helices α_4 and $\alpha_{5'}$ are most flexible secondary elements of the LinB structure. In particular, the maximum amplitude occurred at the end of helix α_4 due to stretching of helix $\alpha_{5'}$, which is supported by the enhanced flexibility of helixes α_4 and $\alpha_{5'}$, especially Glu146 and Asp147 observed in the present study. The molecular dynamics (*23*) also showed that the secondary essential motion was around the Ile138, Pro212, and Ala214 residues participating in the β-bridge formed by hydrogen bonds.

The halogen position in the active center is approximately the same in the all mentioned complex structures. The second Br^- ion is at distance of 16.5 Å from Br^- in the active site in both LinB−PGO and LinB−BPO. It appears that the secondary Br^- ions are in the less dense layer of the enzyme separating two domains (Figure 2) with channels connecting the active center with surface of the protein. This suggests that these Br^- ions originate from the substrate molecules. The active site Br− ion makes hydrogen bonds with two primary halide-stabilizing residues (Asn38 and Trp109) and is in close contact with secondary halide-stabilizing residues (Trp207, Pro208, and Ile211) proposed to play very important role for the catalytic cycle of LinB (*25*).

The observed dehalogenation of 1,2-dibromopropane and 2,3-dibromopropene supports the general trend that the sp^3-hybridized carbon is the predominant electrophilic site for the S_N2 bimolecular neucleophilic substitution in dehalogenation reaction. In respect to the biochemical assays, the X-ray analysis agrees well with the GC-MS identification of the reaction products suggesting that the observed products of the crystalline enzyme are relevant to the enzyme normal metabolic role.

ACKNOWLEDGMENT

Dr. Jaromir Marek (Masaryk University, Brno, Czech Republic) is gratefully acknowledged for providing X-ray data for LinB and LinB-PDO structures. We would like to thank referees for valuable suggestions, especially in regard to biochemical assays.

REFERENCES

1. Holmquist, M. (2000) *Curr. Protein Pept. Sci.* 1, 209−235.
2. Verschueren, K. H. G., Franken, S. M., Rozeboom, H. J., Kalk, K. H., and Dijkstra, B. W. (1993) *J. Mol. Biol. 232*, 856−872.
3. Schanstra, J. P., and Janssen, D. B. (1996) *Biochemistry 35*, 5624−5632.
4. Nagata, Y., Nariya, T., Ohtomo, R., Fukuda, M., Yano, K., and Takagi, M. (1993) *J. Bacteriol. 175*, 6403−6410.
5. Nagata, Y., Miyauchi, K., Damborsky, J., Manova, K., Ansorgova, A., and Takagi, M. (1997) *Appl. Environ. Microbiol. 63*, 3707−3710.
6. Keuning, S., Janssen, D. B., and Witholt, B. (1985) *J. Bacteriol. 163*, 635−639.
7. Janssen, D. B., Pries, F., van der Ploeg, J., Kazemier, B., Terpstra, P., and Witholt, B. (1989) *J. Bacteriol. 171*, 6791−6799.
8. Kulakova, A. N., Larkin, M. J., and Kulakov, L. A. (1997) *Microbiology 143*, 109−115.
9. Damborsky, J., Nyandoroh, M., Nemec, M., Holoubek, I., Bull, A., and Hardman, D. (1997) *Biotechnol. Appl. Biochem. 26*, 19−25.
10. Franken, S. M., Rozeboom, H. J., Kalk, K. H., and Dijkstra, B. W. (1991) *EMBO J. 10*, 1297−1302.
11. Verschueren, K. H. G., Franken, S. M., Rozeboom, H. J., Kalk, K. H., and Dijkstra, B. W. (1993) *J. Mol. Biol. 232*, 856−872.
12. Ridder, I. S., Rozeboom, H. J., and Dijkstra, B. W. (1999) *Acta Crystallogr. D55*, 1273−1290.
13. Newman, J., Peat, T. S., Richard, R., Kan, L., Swanson, P. E., Affholter, J. A., Holmes, I. H., Schindler, J. F., Unkefer, C. J., and Terwilliger, T. C. (1999) *Biochemistry 38*, 16105−16114.
14. Marek, J., Vevodova, J., Kuta-Smatanova, I., Nagata, Y., Svennson, A., Newman, J., Takagi, M., and Damborsky, J. (2000) *Biochemistry 39*, 14082−14086.
15. Oakley, A. J., Prokop, Z., Bohac, M., Kmunicek, J., Jedlicka, T., Monincova, M., Kuta-Smatanova, I., Nagata, Y., Damborsky, J., and Wilce, M. C. J. (2002) *Biochemistry 41*, 4847−4855
16. Damborsky, J., Manova, K., Berglund, A., Sjöström, M., Nemec, M., and Holoubek, I. (1997) *Adv. Environ. Res. 1*, 50−57.
17. Nagata, Y., Miyauchi, K., Damborsky, J., Manova, K., Ansorgova, A., and Takagi, M. (1997) *Appl. Environ. Microbiol. 63*, 3707−3710.
18. Smatanova, I., Nagata, Y., Svensson, L. A., Takagi, M., and Marek, J. (1999) *Acta Crystallogr. D55*, 1231−1233.
19. Otwinowski, Z., and Minor, W. (1997) *Methods Enzymol. 276*, 307−326.
20. Brunger, A. T., Adams, P. D. Clore, G. M., Delano, W. L., Gros, P., Grosse-Kunstleve, R. W., Jiang, J.-S., Kuszewski, J., Nilges, M., Pannu, N. S., Read, R. J., Rice, L. M., Simonson, G. L., and Warren, G. L. (1998) *Acta Crystallogr. D54*, 905−921.
21. McRee, D. E. (1999) *J. Struct. Biol. 125*, 156−165.
22. Kleywegt, G. J., and Jones, T. A. (1994) *Acta Crystallogr. D50*, 178−185.
23. Otyepka, M., and Damborsky, J. (2002) *Protein Sci. 11*, *1206−1217*.
24. Damborsky, J., Berglund, A., Kuty, M., Ansorgova, A., Nagata, Y., and Sjöström, M. (1998) *Quant. Struct.-Act. Relat. 17*, 450−458.
25. Bohac, M., Nagata, Y., Prokop, Z., Prokop, M., Monincova, M., Tsuda, M., Koca, J., and Damborsky, J. (2002) *Biochemistry 41*, 14272−14280.
26. Humphrey, W., Dalke, A., and Shulten, K. (1996) *J. Mol. Graphics 14.1*, 33−38.

BI027280A